PLOS ONE

RESEARCH ARTICLE

Patient-specific modeling of right coronary circulation vulnerability post-liver transplant in Alagille's syndrome

Miguel Silva Vieira[1☯]*, **Christopher J. Arthurs**[1☯], **Tarique Hussain**[2,3], **Reza Razavi**[1,3], **Carlos Alberto Figueroa**[1,4]

1 Division of Imaging Sciences & Biomedical Engineering, King's College London, London, United Kingdom, **2** Department of Pediatrics, University of Texas Southwestern Medical Center at Dallas, United States of America, **3** Pediatric Cardiology Department, Evelina Children's Hospital London, Guy's and St. Thomas' NHS Foundation Trust, London, United Kingdom, **4** Departments of Surgery and Biomedical Engineering, University of Michigan, Michigan, United States of America

☯ These authors contributed equally to this work.
* miguel.silvavieira@kcl.ac.uk

Citation: Silva Vieira M, Arthurs CJ, Hussain T, Razavi R, Figueroa CA (2018) Patient-specific modeling of right coronary circulation vulnerability post-liver transplant in Alagille's syndrome. PLoS ONE 13(11): e0205829. https://doi.org/10.1371/journal.pone.0205829

Editor: Leonidas G. Koniaris, Indiana University, UNITED STATES

Received: February 26, 2018

Accepted: October 2, 2018

Published: November 8, 2018

Data Availability Statement: Supporting Information files are available through the University of Michigan Blue Data Repository: https://doi.org/10.7302/Z2N58JM4. The technical specifications required to reproduce the results obtained in this research are found in the supplementary technical note.

Funding: The authors acknowledge funding from the European Research Council under the European Union's Seventh Framework Programme (FP/2007-2013) / ERC Grant Agreement n. 307532

Abstract

Objectives

Cardiac output (CO) response to dobutamine can identify Alagille's syndrome (ALGS) patients at higher risk of cardiovascular complications during liver transplantation. We propose a novel patient-specific computational methodology to estimate the coronary autoregulatory responses during different hemodynamic conditions, including those experienced in a post-reperfusion syndrome (PRS), to aid cardiac risk-assessment.

Material and methods

Data (pressure, flow, strain and ventricular volumes) from a 6-year-old ALGS patient undergoing catheter/dobutamine stress MRI (DSMRI) were used to parameterize a closed-loop coupled-multidomain (3D-0D) approach consisting of image-derived vascular models of pulmonary and systemic circulations and a series of 0D-lumped parameter networks (LPN) of the heart chambers and the distal arterial and venous circulations. A coronary microcirculation control model (CMCM) was designed to adjust the coronary resistance to match coronary blood flow (and thus oxygen delivery) with MVO2 requirements during Rest, Stress and a virtual PRS condition.

Results

In all three simulated conditions, diastolic dominated right coronary artery (RCA) flow was observed, due to high right ventricle (RV) afterload. Despite a measured 45% increase in CO, impaired coronary flow reserve (CFR) (~1.4) at Stress was estimated by the CMCM. During modeled PRS, a marked vasodilatory response was insufficient to match RV myocardial oxygen requirements. Such exhaustion of the RCA autoregulatory response was not anticipated by the DSMRI study.

to CAF. The authors acknowledge support from the the United Kingdom Department of Health via the National Institute for Health Research (NIHR) comprehensive Biomedical Research Centre award to Guy's & St Thomas' NHS Foundation Trust in partnership with King's College London and King's College Hospital NHS Foundation Trust.

Competing interests: The authors have declared that no competing interests exist.

Abbreviations: ALGS, Alagille's syndrome; DSMRI, Dobutamine stress MRI; CBF, Coronary blood flow; CFR, Coronary flow reserve; CMCM, Coronary microvasculature control model; LCA, Left coronary artery; LCC, Left coronary circulation; LT, Liver transplantation; LV, Left ventricle; MAP, Mean aortic pressure; MVO_2, myocardial oxygen consumption; MRI, Magnetic resonance imaging; RCA, Right coronary artery; RHF, Right heart failure; RV, Right ventricle; PPS, Peripheral pulmonary stenosis; SSFP, Steady-state free precession.

Conclusion

Impaired CFR undetected by DSMRI resulted in predicted myocardial ischemia in a computational model of PRS. This computational framework may identify ALGS patients at higher risk of complications during liver transplantation due to impaired coronary microvascular responses.

Introduction

Alagille's syndrome (ALGS) is a rare autosomal dominant multi-systemic vasculopathy, with variable penetrance and expression, and an estimated incidence of 1:30,000 up to 1:50,000 per liver birth [1,2]. Several mutations have been reported in genes involved in the Notch signaling pathway that regulate differentiation of cell migration during fetal vascular development [3]. These are thought to be the cause of this polymalformative disorder affecting the liver (paucity of interlobular bile ducts resulting in neonatal cholestasis), heart (peripheral pulmonary stenosis, PPS), eyes (posterior embryotoxon), and skeleton (butterfly-like vertebral arch defects), and associated with a characteristic dysmorphic facies. Currently, genetic testing is available and enables non-invasive confirmation since the phenotypic expression of the disease is highly variable [4]. ALGS typically presents in the first 3 to 6 months of life with cholestasis, coursing in half of the cases with debilitating pruritus, disfiguring xanthomas and failure to thrive due to fat malabsorption [4]. Despite aggressive medical care (e.g. tailored diet with carbohydrate, medium-chain triglycerides and individual fat-soluble vitamins supplementation, bile flow stimulants, bile acid–binding resins and antihistamines), in 20–30% of children liver transplantation (LT) is the only option for end-stage liver failure and the debilitating cholestasis symptoms [5].

In general, LT is associated with hemodynamic instability notably during the reperfusion of the allograft due to the sudden release of vasoactive mediators into the systemic circulation [6]. These events, first defined by Aggarwal S et al. [6] in 1987 (post-reperfusion syndrome, PRS) include, on one hand, a decreased in mean arterial pressure (MAP) and systemic vascular resistance (SVR), and on the other hand, an increase in pulmonary arterial pressure (PAP), pulmonary artery wedge pressure (PAWP), and central venous pressure (CVP), in addition to cardiac arrhythmias.

LT in ALGS has been associated with higher risk of complications (early/late mortality and graft failure), particularly during the allograft reperfusion. This increased risk has been ascribed to preexisting cardiopulmonary disease [7]. It has been postulated that PPS, which occurs in over 2/3 of patients, leads to progressive right ventricular (RV) remodeling (compensatory hypertrophy initially and eventually dilation with systolic function impairment). This on one hand, may result in acute right heart failure (RHF) and eventually cardiogenic shock during the critical period of reperfusion and, on the other hand, may prevent a sustained increase in CO normally required to perfuse the transplanted liver [7–11].

Pre-transplant cardiovascular risk assessment through dobutamine stress imaging

A thorough pre-operative cardiac assessment is currently recommended to identify ALGS patients who are likely to be at higher risk because of their cardiovascular disease [12]. Razavi RS et al. [13] have proposed a dynamic method to mimic the hemodynamic conditions of

reperfusion after LT. Using dobutamine as an inotropic vasodilator, they have shown that the patients' hemodynamic response could predict their ability to increase the CO in the immediate post-transplant period to meet the demands of systemic hypotension that occurs with liver reperfusion [12,13]. Although not consensual, it has been proposed that a 40% increase in CO is the required hemodynamic response to the ensuing generalized systemic vasodilation in order to allow a successful liver transplant [12].

The standard protocol uses a two-stage dobutamine infusion (10 μg/kg/min and 20 μg/kg/min). This staged approach allows to assess the response to increasing doses and therefore prevent complications. Razavi RS et al. have described that a significant decrease in the systemic vascular resistance (close to that seen during liver reperfusion) was only observed with the higher dose of 20 μg/kg/min and thus this has been established as the target dose for a diagnostic test.

Pressure-flow autoregulation and coronary flow reserve in ALGS

Under resting physiologic conditions, coronary blood flow (CBF) occurs predominantly during diastole, when intra-myocardial tissue pressure, particularly in the endocardium, falls below the aortic root pressure [14,15].

Notably, normalized resting CBF to the RV, which is significantly lower than that to the left ventricle (LV) due to its lower myocardial oxygen consumption (MVO_2), is not significantly affected by its contraction. Due to lower RV systolic extravascular compressive forces, flow in the right coronary artery (RCA) occurs throughout the cardiac cycle [15,16]. In contrast, flow in the left coronary artery (LCA) flow is predominantly diastolic.

A complex network of integrative pathways not fully understood (metabolic, myogenic and endothelial-dependent), modulates the coronary microcirculation vasomotor tone, exerting a delicate control of the myocardial perfusion so that there is a close match between oxygen delivery and changes in MVO_2 [17,18]. Myocardial perfusion is directly proportional to the pressure gradient across the coronary circulation and inversely proportional to coronary resistance. Given the heart's limited anaerobic capacity and oxygen extraction reserve, notably reduced in RV pressure overload, often seen in ALGS patients, coronary vasodilation in response to inadequate myocardial oxygen delivery is critical to mitigate ischemic injury [15,19]. Despite a high degree of coronary microcirculation autoregulation, there is a threshold below which a further fall in the aortic perfusion pressure (e.g. during PRS) cannot be compensated by an additional decrease in coronary resistance. Moreover, the coronary vasodilator reserve appears to be lower in the RCA territory [20].

During physiological autoregulation, CBF changes in response to a decrease in MAP are the result of both a reduced perfusion pressure and a reduced MVO_2, consequence of a lower LV afterload. This strong coupling between CBF and MVO_2 makes it difficult to study in-vivo complex coronary pressure-flow autoregulation mechanisms and isolate their individual contributions [15].

ALGS patients classically present some form of pulmonary vasculopathy (over 2/3 have PPS) [1,2]. As in other pulmonary vasculopathies, structural remodeling (stiffening) of the pulmonary arteries walls results in increased RV afterload and compensatory hypertrophy leading to a restrictive physiology [21]. Although to our knowledge no data is available in ALGS children, we hypothesize that with increasing RV wall tension and consequently $RVMVO_2$, there is a progressive shift of RCA flow to diastole, rendering it more LCA-like. Van Wolferen SA et al. [22] have demonstrated in an MRI study that adults with pulmonary hypertension have systolic RCA flow impediment proportional to RV pressure and mass. This could predispose to RV ischemia and contribute to RV failure seen in some patients. In ALGS children with

near-systemic RV pressures, a similar scenario may occur, with compression of the intramyocardial microvasculature reducing the perfusion gradient between the aorta and RCA bed and flow impairment occurring potentially even before the vasodilator reserve is exhausted [22–24]. This may increase the risk of RV ischemia and RHF during the dramatic cardiovascular and metabolic derangements of liver reperfusion, when the coronary perfusion pressure is further decreased [25].

Rationale for the present study

We submit that the dobutamine stress test does not account for all key hemodynamic events during liver transplantation: while the test might reproduce the increase in heart rate and myocardial metabolic demand, it fails to account for the systemic vasodilation and corresponding coronary perfusion pressure drop during transplantation [26]. Furthermore, the general guideline of 40% increase in CO during dobutamine stress MRI (DSMRI) might not guarantee adequate RCA perfusion during post-reperfusion syndrome (PRS).

In this study, we propose to use computational modeling to shed some light into RCA hemodynamics during PRS, in combination with image-based and catheterization data on two subject-specific hemodynamic stages in an ALGS subject. Towards that, we study three different conditions:

1. *Rest* condition, in which a computational model of RV, LV, RCA, LCA, aorta, and pulmonary arteries is calibrated to reproduce baseline hemodynamic data for the patient.
2. *Stress* condition, in which the computational model above is adjusted to reproduce hemodynamic conditions during DSMRI for the same patient.
3. *PRS* condition, entirely computational, in which the Stress condition is further modified to account for the systemic pressure drop during PRS.

This framework can be used to study coronary flow reserve (CFR) and assess possible shortcoming of the DSMRI test.

Material and methods

Ethical approval was obtained from St. Thomas' Hospital Research Ethics Committee/South East London Research Ethics Committee (10/H0802/65).

1. Catheter and magnetic resonance imaging study

Data was collected from a 6-year-old ALGS patient undergoing a hybrid X-ray catheter/DSMRI study as described previously [27]. Combined acquisition of functional (flow and volumes) at rest and peak dobutamine stress (20 μg/kg/minute) and three-dimensional (3D) morphologic MRI data (dual-phase), with concomitant central pressure monitoring, was performed and used to parameterize the computational simulations. Images were acquired using a 1.5T MR-scanner (Achieva, Philips, Best, Netherlands) and a Philips BV Pulsera cardiac X-Ray unit under general anesthesia, which was maintained constant throughout the procedure. Details of the imaging parameters are provided in Table A in S1 File.

2. Patient-specific computational modeling simulation of hemodynamics

A novel modeling framework that integrates image data and detailed invasive/non-invasive measurements was used to obtain a faithful computational representation of the patient's

physiology. A brief description of key aspects of the model is provided in the following sections (further details are available in the Technical Note in S1 File).

2.1. Fluid-solid interaction models of the aorta and pulmonary arteries. The CRIMSON custom software (CardiovasculaR Integrated Modeling and SimulatiON; http://www.crimson.software/) was used to segment the aorta and main branches, including the coronaries, and the central pulmonary arteries, using a semi-automatic segmentation method to produce an analytical representation of the vessels (Fig 1) from the diastolic phase of the 3D-Steady-state free precession (SSFP) sequence. Details regarding this segmentation approach are found elsewhere [28]. The 3D geometry was discretized into a volumetric finite element mesh consisting of 1,687,949 tetrahedral elements (characteristic dimension h = 0.8mm) and 325,463 nodes, with curvature-based refinement.

Blood was modeled as an incompressible Newtonian fluid (density ρ = 0.00106 g/mm^3 and viscosity μ = 0.004g/mm·s). Blood vessels were modeled using the Coupled Momentum Method, whereby an incompressible linear elastic membrane with spatially-varying structural stiffness is monolithically-coupled to the fluid domain [29]. The linearized stiffness (E) of the aorta, its branches, and the central pulmonary arteries were prescribed according to the equation:

$$E = \frac{P_{syst} - P_{diast}}{D_{syst} - D_{diast}} \times D_{diast} \times h$$

where P_{syst} and P_{diast} represent the catheter-derived systolic and diastolic pressures, respectively, and D_{syst} and D_{diast} the 3D-SSFP-derived systolic and diastolic diameters at the level of the aortic and pulmonary artery roots, respectively. Wall thickness was prescribed to be 1 mm throughout. This produced a linearized stiffness of 2.26 x 10^5 g/mm·s^2 for the systemic and 1.30 x 10^5 g/mm·s^2 for the pulmonary arteries.

2.2. Coupled multidomain model. Expanding on previous developments by our group [30], we have designed a closed-loop coupled-multidomain (3D-0D) model consisting of image-based portions of the pulmonary and systemic circulations (where image data was available), and LPN (0D) models of the heart chambers and the arterial and venous distal circulations (see Fig 1). Parameter values for the LPN models for each condition are given in Tables B-F of the Technical Note in S1 File.

2.3. OD coronary microvascular control model (CMCM). Metabolic control of the coronary microcirculation was achieved using a method develop by our group, which has been tested against invasive patient data [18]. The foundation of this LPN model relies on using CBF as a surrogate of myocardial oxygen delivery [18], and on dynamically adapting coronary microvascular resistance to eliminate any "myocardial hunger" (i.e. mismatch between oxygen demand and supply). The myocardial oxygen demand per heartbeat was computed from the cardiac workload, determined by the 0D heart model, after integrating the area of the ventricular pressure-volumes curves and the ventricular elastance function. Because the CMCM can reproduce patient coronary vasomotor responses to changes in cardiac workload, it has the ability to predict CBF adaptations in response to changes in the myocardial oxygen demand and coronary perfusion pressure gradient. This permits simulation of the coronary response to a generalized vasodilation state as seen during liver reperfusion and enables specific probing of the complex coronary microcirculatory responses.

The model assumed a fixed oxygen extraction of 40% and 80% for the RCA and LCA respectively at Rest and 100% for both coronary circulations at Stress [15,20].

2.4. RV and LV elastance functions. RV and LV elastance functions were derived from ventricular cines and catheterization data, describing cyclic ventricular volume and

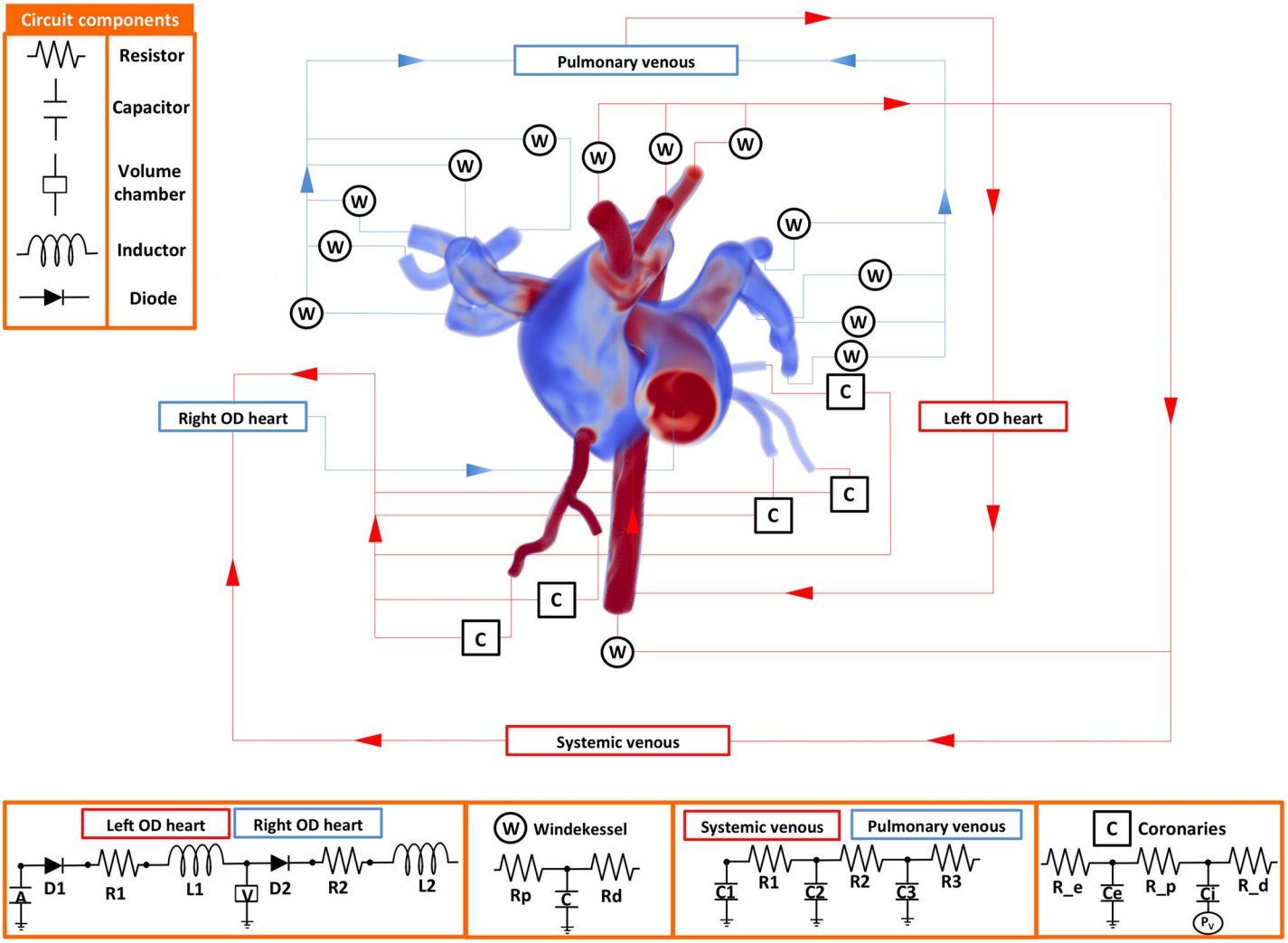

Fig 1. Patient-specific closed-loop model used to simulate pulsatile hemodynamics coupling lumped parameter networks (LPN, 0D) and image-based (3D) vascular models. The model includes: LV (0D), aorta, coronary arteries and major branches (3D), medium and small systemic arteries (0D), arterioles (0D), venules (0D), veins (0D), right atrium (0D), RV (0D), pulmonary arteries up to second generation branching (3D), small pulmonary arteries (0D), arterioles (0D), venules (0D), veins (0D) and left atrium (0D). P_v represents the node where the broadcasted intraventricular pressure was transmitted as described by Arthurs et al (2013) [18]. Details of the parameters used for each component can be found in the Technical Note in S1 File.

https://doi.org/10.1371/journal.pone.0205829.g001

intraventricular pressures, respectively, using methods described in Arthurs et al [18]. Ventricular volume curves, obtained by manually contouring the endocardial borders of all cardiac phases of the cardiac MRI short-axis cines, were matched with the corresponding R-wave in the invasive pressure recordings to obtain time-varying elastance functions (further details in the Technical Note in S1 File). Ventricular volumetric parameters for the Rest and Stress conditions used to define their corresponding elastance functions are listed in Table 1.

2.5. Additional specifications for the experimental conditions. At peak DSMRI, cardiac output increased by ~45% from baseline. No regional wall motion abnormalities were noted. Tissue stiffness was kept constant through all three experimental conditions. The PRS condition was defined by imposing a 31% drop in MAP relative to the Stress condition, following Hilmi et al. [10] definition of significant PRS.

Table 1. RV and LV volumetric parameters for Rest and Stress conditions.

Condition	Heart Rate (bpm)	Mass index (g/m^2)		EDV[a] (ml/m^2)		ESV[b] (ml/m^2)		EF[c] (%)	
		LV	RV	LV	RV	LV	RV	LV	RV
Rest	73	54.2	59.8	81	90	35	44	60	51
Stress	106			80	95	23	37	71	61

[a]EDV, end-diastolic volume.

[b]ESV, end-systolic volume.

[c]EF, ejection fraction

https://doi.org/10.1371/journal.pone.0205829.t001

All simulations were performed in our custom parallel blood flow solver CRIMSON using 128 processors on a SGI Altix UV, using a total simulation time of 150 hours per case.

Results

Good agreement (< 6% discrepancy) between the clinical and simulated flow and pressure data was achieved (Fig 2). Tables 2 and 3 summarize relevant hemodynamic results from the simulation. Fig 3 depicts the LV/RV pressure-volume loops (PVL) computed for each condition. The PVL area was used to calculate the cardiac workload and MVO_2 that are shown in Table 2. At Rest, $LVMVO_2$ was just 6% higher than $RVMVO_2$. At Stress, $RVMVO_2$ was 12% higher than $LVMVO_2$.

Table 3 shows several coronary indices computed from the simulation. The CMCM predicted a 1.4-fold increase in CBF with DSMRI (CFR ~ 1.4), followed by a 1.9-fold decrease during transplant PRS. Fig 4 illustrates the interplay between LV/RV pressures and coronary waveforms. In all three conditions, the coronary perfusion occurred mostly during diastole, except for LCA flow for the PRS condition. Diastolic RCA flow dominated, even at Rest. This RCA biphasic profile became more prominent during Stress and PRS conditions, with a dominant diastolic phase, marked systolic flow reversal, and higher peak diastolic-to-systolic flow ratios.

Fig 5 presents the time-averaged 3D maps of pressure, velocity and wall shear stress (WSS) (central panel) and waveforms of aortic and ventricular pressure, as well as right and left coronary flows and pressures (left and right panels). In all three conditions, RCA mean velocity and WSS maps display higher values than in the LCA (see also the Movie in S2 File).

At Rest, coronary resistance was higher in the LCA than in the RCA by just 2%. During Stress, the 39% and 44% drop in LCA and RCA resistance, respectively, was sufficient to match the MVO_2 demands as shown in Fig 6. However, despite a dramatic vasodilatory response in the RCA during PRS condition, with a 76% reduction in resistance, the CMCM predicted insufficient myocardium oxygen delivery (i.e. myocardial hunger). In turn, the LCA autoregulation predicted a 64% fall in resistance, which was sufficient to counter the supply/demand mismatch after a brief period of ischemia.

Discussion

The value of image-based modeling

In-vivo assessment of coronary autoregulation is complex, requiring invasive methodologies that are generally unsuitable for use in patients. Furthermore, the interplay of coordinated control mechanisms present in the coronary microvasculature make computational modeling an appealing prospect for assessing transient events following liver transplantation such as

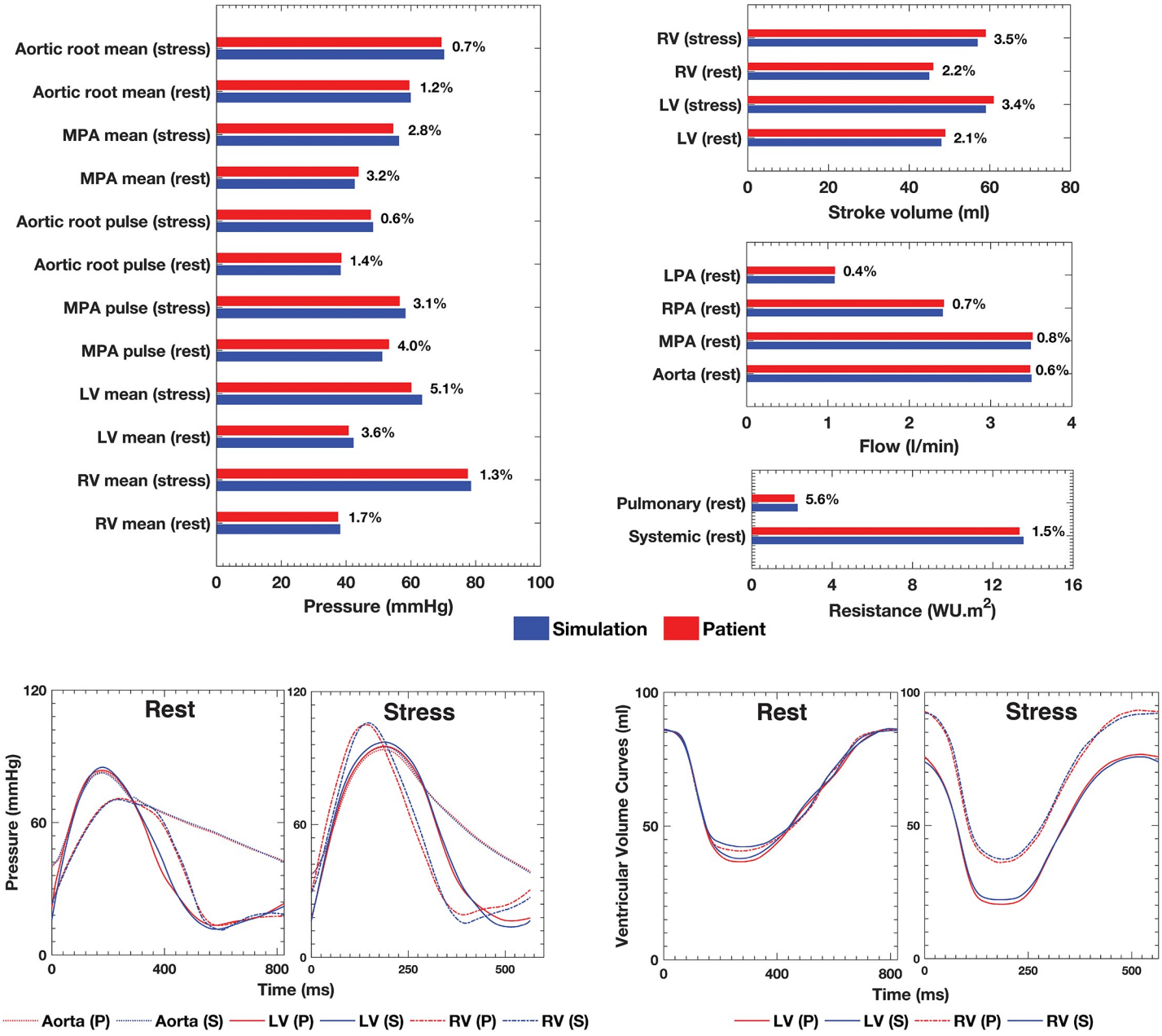

Fig 2. Relative error between patient and simulation data given as a percentage. Bar plots comparing the clinical pressure and flow at relevant anatomic landmarks, and ventricular stroke volume and systemic and pulmonary vascular resistance data at Rest and Stress, and corresponding simulation results. Selected pressures and ventricular volumes transient waveforms corresponding to the cycle-to-cycle equilibrium for the Rest and Stress Conditions are also show. P, patient clinical data. S, simulation results.

https://doi.org/10.1371/journal.pone.0205829.g002

PRS, a serious intraoperative hemodynamic complication associated with significant morbidity and mortality [10]. DSMRI is performed in ALGS patients to assess cardiac risk before liver transplantation. However, while the test might reproduce increases in heart rate and myocardial metabolic demand, it fails to account for the systemic vasodilation and associated coronary perfusion pressure drop during transplantation [26]. Expanding upon previous work [18,29,30], in this study, we used computational modeling to investigate coronary

Table 2. Simulation results of cardiac workload and MVO_2.

Condition	Cardiac workload (J)		MVO_2 (ml/min)	
	LV	RV	LV	RV
Rest	4.6×10^{-1}	3.5×10^{-1}	5.42	5.10
Stress	5.2×10^{-1}	7.2×10^{-1}	6.97	7.93
PRS	2.7×10^{-1}	4.9×10^{-1}	4.39	8.91

https://doi.org/10.1371/journal.pone.0205829.t002

hemodynamics and MVO_2 during PRS, in combination with image-based and catheterization data under Rest and Stress conditions in an ALGS subject.

Study findings

There is a scarcity of data on coronary vasodilatory response to pharmacological stress in children, and to our knowledge, no data available in ALGS children. In a small study using positron emission tomography and adenosine stress perfusion, Muzik et al. [31] reported that CFR is impaired in children post-Kawasaki disease compared to healthy volunteers (3.2±0.7 vs 4.6 ±0.9, respectively). Our computational results showed a much smaller hyperemic CBF response to pharmacological stress (CFR ~ 1.4), notwithstanding an adequate increase in cardiac output elicited by DSMRI. In our study, hyperemic CBF was measured using a different pharmacological agent. Dobutamine, a sympathomimetic amine acting on α/β-adrenoceptors, induces both a positive chronotropic/inotropic response and increases CBF through a metabolic-mediated vasodilation. Whilst the use of an A_2A receptor agonist such as adenosine is the gold standard for inducing hyperemia, dobutamine assesses the cardiac output response, enabling a more physiological approach for studying demand ischemia. Moreover, adenosine can have vasodilatory effects in the pulmonary vascular bed, affecting RV afterload and consequently $RVMVO_2$ and CBF [32].

$LVMVO_2$ was slightly higher (6%) than $RVMVO_2$ at Rest (Table 2). This pattern was reversed during Stress ($LVMVO_2$ was 12% lower than $RVMVO_2$) observed after prescribing a 31% increase in heart rate. These observations reflect high RV afterload and are highly pathological. Nevertheless, the CMCM indicated lack of myocardial hunger (Fig 6) through a significant reduction in RCA resistance. During Stress, the RCA flow profile became even more diastolically dominant, reflecting increased systolic compression of the microvasculature. Due to high RV afterload (1.14:1 systolic RV/ aortic pressure ratio) and compensatory hypertrophy (0.91:1 LV-to-RV normalized mass ratio), the RCA Stress diastolic/systolic CBF ratio (2.5:1) was higher than that of the LCA (2.7:1). Additionally, the vasodilatory response during Stress was more prominent in the RCA (44%) than in the LCA (39%). These microcirculatory events

Table 3. Simulation results of coronary hemodynamics including average CBF, coronary resistance and WSS.

Condition	Coronary blood flow (ml/min/g)		Diastolic/systolic flow ratio		Coronary Resistance ($WU.m^2$)		Coronary WSS ($dyn{\cdot}cm^2$)	
	LCA	RCA	LCA	RCA	LCA	RCA	LCA	RCA
Rest	66.2	67.6	1.8:1 (36.8:29.4)	1.9:1 (35.6:32.0)	1.07×10^2	1.05×10^2	2.82	5.20
Stress	88.3	93.4	2.5:1 (53.0:35.3)	2.7:1 (58.8:34.6)	6.50×10^1	5.83×10^1	5.33	24.18
PRS	51.5	44.6	0.7:1 (15.4:36.1)	2.1:1 (23.4:21.2)	2.36×10^1	1.42×10^1	3.34	15.61

https://doi.org/10.1371/journal.pone.0205829.t003

suggest that the calibrated CMCM LPN could describe the capillary density inadequacy in patients with RV hypertrophy [33].

We adopted the concept of myocardial hunger [18] to simulate the myocardial demand/supply perfusion mismatch (i.e. ischemia). By assuming a fixed 100% oxygen extraction, the metabolic demand during Stress and PRS was entirely dependent on the CMCM adjustments of microvascular resistances, thus favoring sensitivity over specificity for detecting RV hunger. Of course, there is a minimum physiologically achievable microvascular tone. Based on limited available data [31], we set achievable values for microvasculature resistance (see Table F of the Technical Note in S1 File) that are likely below physiological minima. This means that if we see hunger in the model, we would expect that the myocardial oxygen supply would be insufficient clinically. However, the converse is not necessarily true. In our simulations, the RCA territory vasodilatory response in Stress was sufficient to avoid myocardial hunger. However, in the PRS condition, in the face of the significant drop in MAP (31%), the reduced coronary driving pressure and exhausted vasodilatory reserve (76% resistance decrease) resulted in inadequate post-transplant myocardial perfusion, not anticipated by the DSMRI. Our work suggests that due to abnormal ventriculo-arterial-coronary coupling, RCA flow impairment in this ALGS patient, could limit the RV's ability to adapt to the hemodynamic changes during liver reperfusion. To the best of our knowledge, there is no specific research addressing this issue in ALGS children.

Clinical significance

Although several modeling assumptions and simplifications were needed, this study provides a detailed snapshot how CFR impairment in ALGS patients may restrict their ability to adapt to dramatic peri-operative loading changes post-liver transplant. This impaired vasodilatory reserve may be an unrecognized factor determining the immediate and long-term post-transplant outcomes. Our model also emulates coupled ventricular-vascular maladaptations occurring in ALGS that not only increase $RVMVO_2$ but also impose an additional burden on the

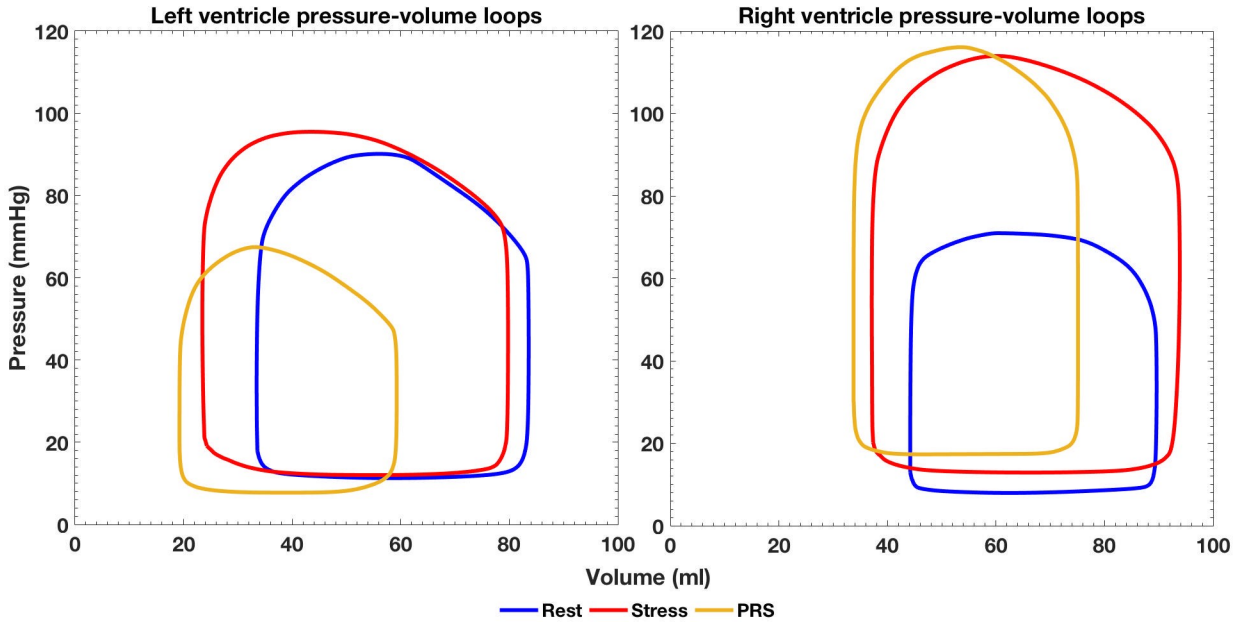

Fig 3. Left and right ventricle pressure-volume loops for the three simulated conditions.

https://doi.org/10.1371/journal.pone.0205829.g003

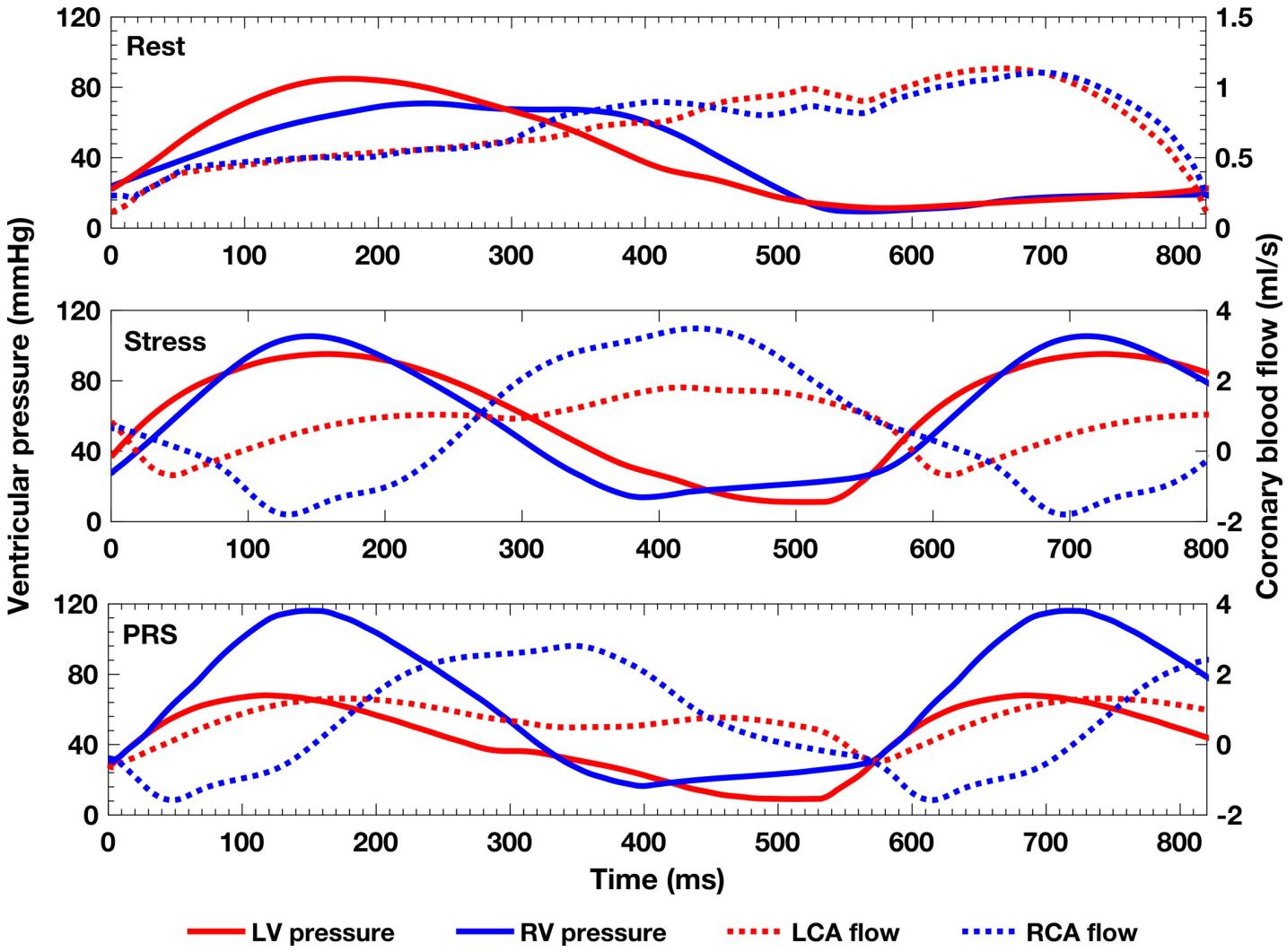

Fig 4. Left and right coronary flow waveforms and ventricular pressure for all three simulated conditions. Different y-axis scales were used in the Rest and Stress/PRS Conditions to best convey the waveforms pulsatility.

https://doi.org/10.1371/journal.pone.0205829.g004

coronary microcirculation autoregulation. We hypothesize that by detecting CFR impairment we could identify a subgroup of patients that despite adequate cardiac output increase with dobutamine stress are at higher risk of cardiac complications post liver reperfusion and could benefit from meticulous optimization of the pre-transplant care (e.g. early diagnosis and endovascular treatment of PPS before RV remodeling; periodic assessment of RV function and size with a MRI; limiting ischaemia–reperfusion injury during organ harvesting) and post-transplant care (e.g. strict hemodynamic monitoring, tailored management of pharmacologic interventions such as vasoactive drugs administration and volume therapy to avoid hypovolemia, as well as excessive cardiac filling resulting in pulmonary edema and deterioration of gas exchange).

Despite the wealth of evidence from experimental animal studies, there is limited patient data available on coronary microvascular pathophysiology and abnormal ventricular-arterial-coronary coupling. Furthermore, because of technical challenges and limitations of in-vivo human studies, the role of reserve exhaustion in the coronary microvasculature in the

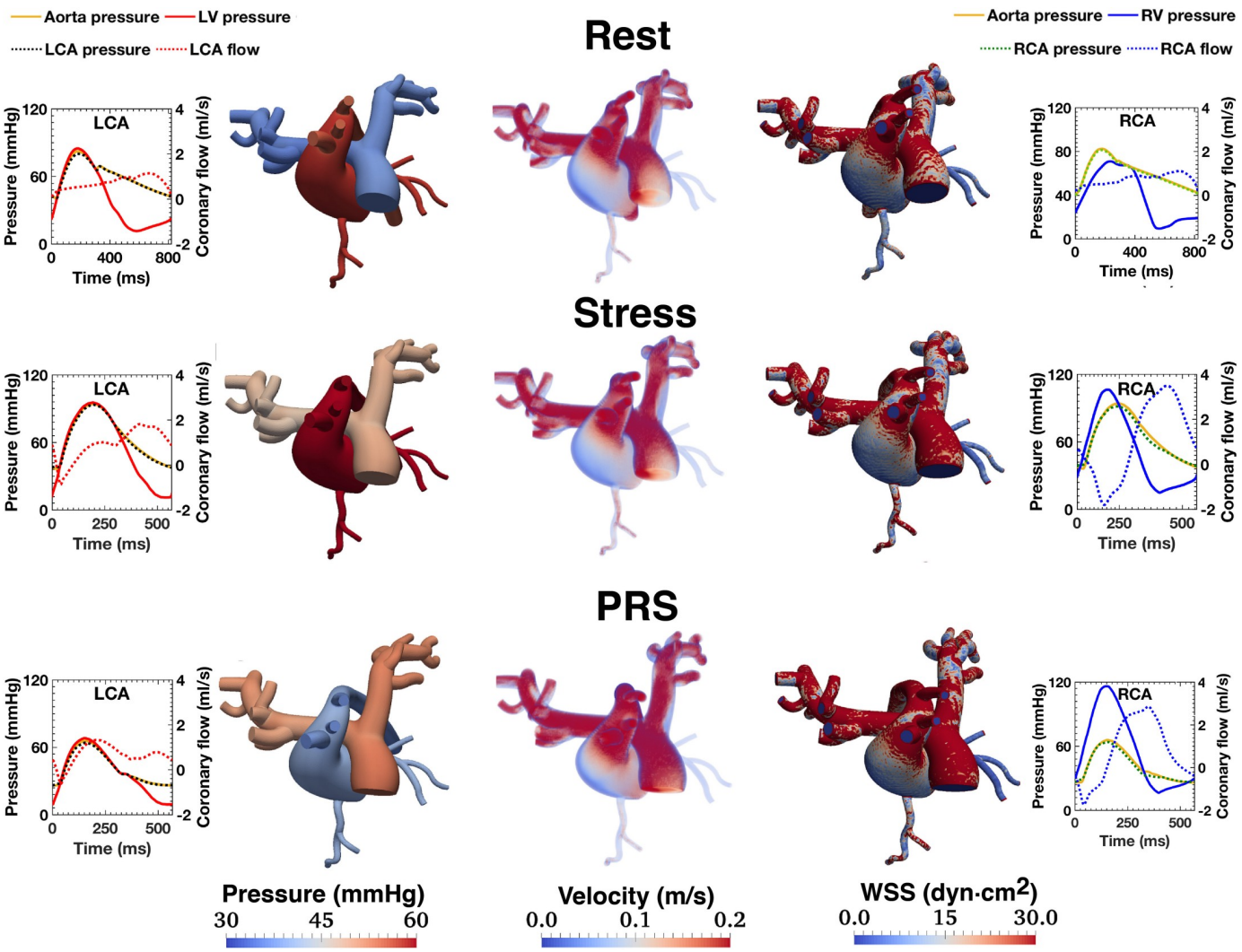

Fig 5. Time averaged maps of pressure, velocity and wall shear stress (WSS) (central panel) and selected flow and pressure waveforms (right and left panels). Notably, mean velocities and WSS in the RCA are higher than in the LCA. See also the Figure in S4 File with instantaneous 3D maps of pressure, velocity and wall shear stress (WSS) at peak systole and peak diastole.

https://doi.org/10.1371/journal.pone.0205829.g005

evolution of diseases that course with chronic increased RV afterload and eventually progress to RV failure is unclear [34]. In patients with pulmonary arterial hypertension, a far common disease, research suggests that increased RV pressure afterload impairs RCA flow and thus myocardial perfusion [22,35], increasing the risk of RV failure [24]. The ultimate validation of our work would require acquisition of CBF data in ALGS children undergoing LT, which is ethically and clinically unfeasible. However, the use of a patient-specific framework of coronary microcirculation such as the one presented, adequately parameterized at baseline and during dobutamine stress to replicate the patient's hemodynamics, has enabled us to simulate the possible pathophysiological events in the coronary microcirculation during LT, for which it is nearly impossible to obtain such data. These results may then help us to pre-operatively identify ALGS subjects who are at risk of developing RV failure.

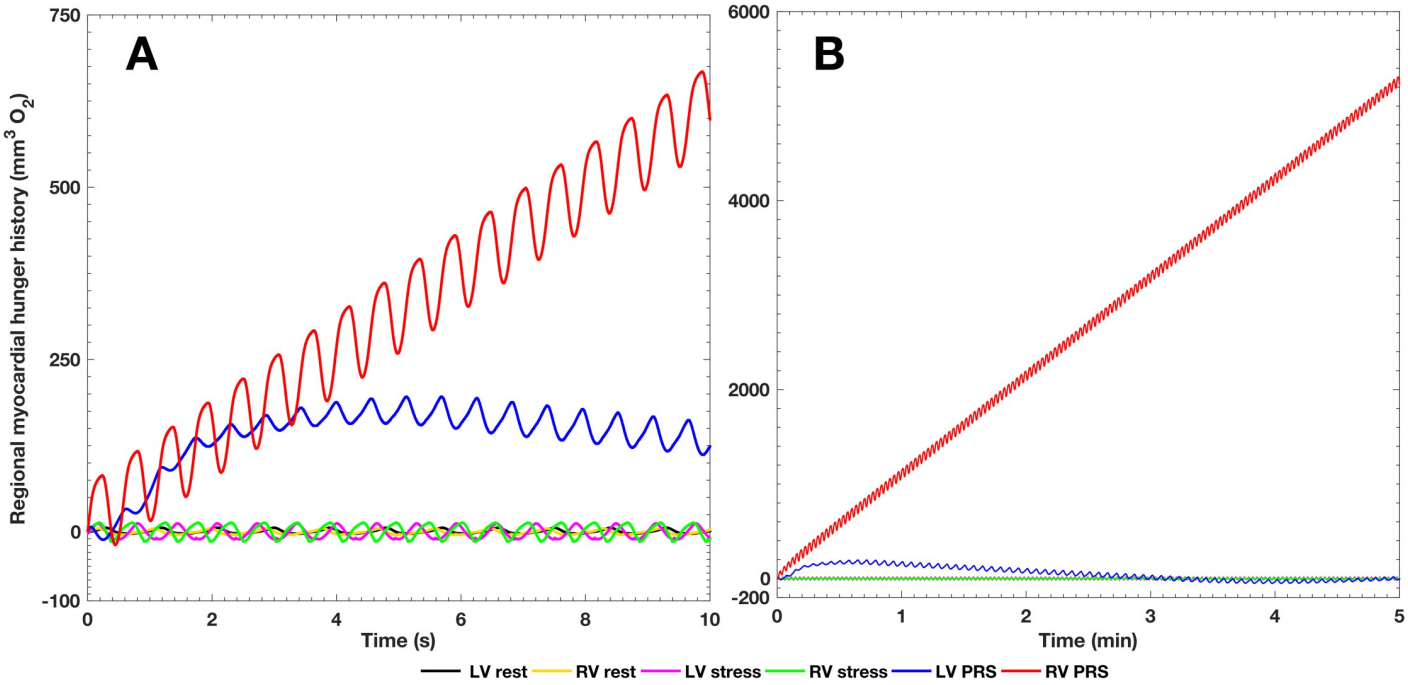

Fig 6. Myocardial oxygen demand/supply mismatch (myocardial hunger) for all three conditions. Panel A: Ten seconds of high-resolution results obtained with the multi-scale 3D-0D model. **Panel B:** A longer simulation time (five minutes) obtained with a reduced-order (0D) model reveals an ever increasing RV myocardial hunger and normalization of LV hunger in the long term.

https://doi.org/10.1371/journal.pone.0205829.g006

Study limitations

Several limitations need to be acknowledged. The expertise required and the computational cost of the proposed image-based computational model hinders its widespread clinical adoption. Although the results of this paper have been calibrated for the Rest and Stress conditions, the lack of data for the PRS condition makes validation difficult. Therefore, we had to rely on arbitrary estimates of the physiologic limit of the coronary microcirculation vasodilatory response and maximal oxygen extraction. The fluid-structure interaction model utilized in this work relies on a small deformation assumption. While this simplification reduces the computational cost, the deformations of the pulmonary tree and the aorta are such that alternative formulations for large structural displacements might be needed. Interventricular dependence has been noted to be important in pulmonary hypertension patients, with increased RV afterload potentially limiting LV filling. Our heart model did not include this dependence and thus there was no pressure feedback between ventricles. However, we assumed that the results of the virtual PRS Condition are realistic because the computational model was fine-tuned to replicate the patient's clinical data at Rest and Stress Conditions, for which we had detailed data. This interdependence element could be included in future designs of the LPN heart model in a similar fashion to that described by Arthurs CJ et al. for the CMCM. There, the changes in cardiac workload and metabolic demands estimated from the pressure-volume loops were "broadcast" to the LPN coronary resistors so that a mathematical model therein could attempt to enforce matching of oxygen supply and demand. A potential model that could be used here would be to impose a threshold in the right intraventricular pressure above which this would modify the left heart elastance function to cause LV underfilling. This would likely further reduce the coronary perfusion during PRS.

Finally, the ultimate goal of this manuscript was to demonstrate the application of an image-based methodology to an ALGS patient in order to study potential pathophysiologic responses following PRS, a problem for which it is difficult to acquire in-vivo data. As such, this manuscript is focused on the methodology and the hypothesis generation, and not on obtaining statistical metrics on a larger patient cohort.

Conclusion

To the best of our knowledge this is the first computational effort to examine altered hemodynamics in ALGS patients. Our model revealed how impaired CFR may restrict adaptive responses in face of reduced aortic perfusion pressure such as that occurring immediately post-transplant. Impaired CFR is likely to result in significant RV myocardial oxygen supply/demand imbalance and could be related to worsened ALGS survival post-transplant. This novel patient-specific experimental computational model can be used to gain insight into the impaired vasoregulatory mechanisms in ALGS, as well as other pulmonary vasculopathies, and aid pre-hepatic transplant cardiac risk stratification. In the future, the predictions of this model could be tested by studying the correlation between outcomes in ALGS patients following liver transplant and MRI quantifications of RCA and LCA flows.

Supporting information

S1 File. Technical note. Description the MRI imaging parameters used, the mathematical model design, the parameterization methods and parameter values, as well as the modeling assumptions made during the study.
(DOCX)

S2 File. Movie. Volume-rendered, time and spatially varying vascular hemodynamics of the three simulated conditions.
(MP4)

S3 File. Figure. 3D geometry of the aorta and main branches, including the coronaries, and the central pulmonary arteries, segmented from the 3D-SSFP MRI sequence.
(TIF)

S4 File. Figure. Instantaneous 3D maps of pressure, velocity and wall shear stress (WSS) at peak systole and peak diastole.
(TIF)

Author Contributions

Conceptualization: Miguel Silva Vieira, Christopher J. Arthurs, Carlos Alberto Figueroa.

Data curation: Miguel Silva Vieira, Tarique Hussain, Carlos Alberto Figueroa.

Formal analysis: Miguel Silva Vieira, Christopher J. Arthurs, Carlos Alberto Figueroa.

Funding acquisition: Carlos Alberto Figueroa.

Investigation: Miguel Silva Vieira, Christopher J. Arthurs, Tarique Hussain, Reza Razavi, Carlos Alberto Figueroa.

Methodology: Miguel Silva Vieira, Christopher J. Arthurs, Carlos Alberto Figueroa.

Project administration: Reza Razavi, Carlos Alberto Figueroa.

Resources: Miguel Silva Vieira, Tarique Hussain, Reza Razavi, Carlos Alberto Figueroa.

Software: Christopher J. Arthurs, Carlos Alberto Figueroa.

Supervision: Christopher J. Arthurs, Tarique Hussain, Reza Razavi, Carlos Alberto Figueroa.

Validation: Miguel Silva Vieira, Christopher J. Arthurs, Carlos Alberto Figueroa.

Visualization: Miguel Silva Vieira, Christopher J. Arthurs, Carlos Alberto Figueroa.

Writing – original draft: Miguel Silva Vieira.

Writing – review & editing: Miguel Silva Vieira, Christopher J. Arthurs, Tarique Hussain, Reza Razavi, Carlos Alberto Figueroa.

References

1. Alagille D, Estrada A, Hadchouel M, Gautler M, Odièvre M, Dommergues JP. Syndromic paucity of interlobular bile ducts (Alagille syndrome or arteriohepatic dysplasia): Review of 80 cases. *J Pediatr*. 1987. https://doi.org/10.1016/S0022-3476(87)80153-1
2. Emerick KM, Rand EB, Goldmuntz E, Krantz ID, Spinner NB, Piccoli DA. Features of Alagille syndrome in 92 patients: Frequency and relation to prognosis. *Hepatology*. 1999. https://doi.org/10.1002/hep.510290331 PMID: 10051485
3. Turnpenny PD, Ellard S. Alagille syndrome: pathogenesis, diagnosis and management. *Eur J Hum Genet*. 2012. https://doi.org/10.1038/ejhg.2011.181 PMID: 21934706
4. Kamath BM, Baker A, Houwen R, Todorova L, Kerkar N. Systematic Review: the Epidemiology, Natural History and Burden of Alagille Syndrome. *J Pediatr Gastroenterol Nutr*. 2018. https://doi.org/10.1097/MPG.0000000000001958 PMID: 29543694
5. Kamath BM, Loomes KM, Piccoli DA. Medical management of alagille syndrome. *J Pediatr Gastroenterol Nutr*. 2010. https://doi.org/10.1097/MPG.0b013e3181d98ea8 PMID: 20479679
6. Aggarwal S, Kang Y, Freeman JA, Fortunato FL, Pinsky MR. Postreperfusion syndrome: cardiovascular collapse following hepatic reperfusion during liver transplantation. *Transpl Proc*. 1987; 19(4 Suppl 3):54–55. https://www.ncbi.nlm.nih.gov/pubmed/3303534.
7. Arnon R, Annunziato R, Miloh T, Suchy F, Sakworawich A, Sogawa H, et al. Orthotopic liver transplantation for children with Alagille syndrome. *Pediatr Transpl*. 2010. https://doi.org/10.1111/j.1399-3046.2009.01286.x PMID: 20070561
8. Png K, Veyckemans F, De Kock M, Carlier M, Sluysmans T, Otte JB, et al. Hemodynamic changes in patients with Alagille's syndrome during orthotopic liver transplantation. *Anesth Analg*. 1999. https://doi.org/10.1097/00000539-199911000-00011
9. Tzakis AG, Reyes J, Tepetes K, Tzoracoleftherakis V, Todo S, Starzl TE. Liver Transplantation for Alagille's Syndrome. *Arch Surg*. 1993. https://doi.org/10.1001/archsurg.1993.01420150093017
10. Hilmi I, Horton CN, Planinsic RM, Sakai T, Nicolau-Raducu R, Damian D, et al. The impact of postreperfusion syndrome on short-term patient and liver allograft outcome in patients undergoing orthotopic liver transplantation. *Liver Transplant*. 2008. https://doi.org/10.1002/lt.21381 PMID: 18383079
11. de la Morena G, Acosta F, Villegas M, Bento M, Sansano T, Bueno FS, et al. Ventricular function during liver reperfusion in hepatic transplantation. A transesophageal echocardiographic study. *Transplantation*. 1994.
12. Squires RH, Ng V, Romero R, Ekong U, Hardikar W, Emre S, et al. Evaluation of the pediatric patient for liver transplantation: 2014 practice guideline by the American Association for the Study of Liver Diseases, American Society of Transplantation and the North American Society for Pediatric Gastroenterology, Hepatolo. *Hepatology*. 2014; 60(1):362–398. https://doi.org/10.1002/hep.27191 PMID: 24782219
13. Razavi RS, Baker A, Qureshi SA, Rosenthal E, Marsh MJ, Leech SC, et al. Hemodynamic response to continuous infusion of dobutamine in Alagille's syndrome. *Transplantation*. 2001. https://doi.org/10.1097/00007890-200109150-00014
14. Hoffman JI, Spaan J a. Pressure-flow relations in coronary circulation. *Physiol Rev*. 1990. https://doi.org/10.1152/physrev.1990.70.2.331 PMID: 2181499
15. Tune JD. *Coronary Circulation (Colloquium Series on Integrated Systems Physiology: From Molecule to Function to Disease*. 1st Ed. San Rafael, Calif.: Morgan & Claypool Life Sciences; 2014. https://doi.org/10.1016/B978-0-323-08697-4.00011–3

16. Lowensohn HS, Khouri EM, Gregg DE, Pyle RL, Patterson RE. Phasic right coronary artery blood flow in conscious dogs with normal and elevated right ventricular pressures. *Circ Res*. 1976. https://doi.org/10.1161/01.RES.39.6.760
17. Tune JD, Gorman MW, Feigl EO. Matching coronary blood flow to myocardial oxygen consumption. *J Appl Physiol*. 2004. https://doi.org/10.1152/japplphysiol.01345.2003 PMID: 15220323
18. Arthurs CJ, Lau KD, Asrress KN, Redwood SR, Figueroa CA. A mathematical model of coronary blood flow control: simulation of patient-specific three-dimensional hemodynamics during exercise. *Am J Physiol—Hear Circ Physiol*. 2016. https://doi.org/10.1152/ajpheart.00517.2015 PMID: 26945076
19. Wong YY, Ruiter G, Lubberink M, Raijmakers PG, Knaapen P, Marcus JT, et al. Right ventricular failure in idiopathic pulmonary arterial hypertension is associated with inefficient myocardial oxygen utilization. *Circ Hear Fail*. 2011. https://doi.org/10.1161/CIRCHEARTFAILURE.111.962381 PMID: 21900188
20. Zong P, Tune JD, Downey HF. Mechanisms of oxygen demand/supply balance in the right ventricle. *Exp Biol Med*. 2005. https://doi.org/10.1177/153537020523000801
21. Inuzuka R, Seki M, Sugimoto M, Saiki H, Masutani S, Senzaki H. Pulmonary arterial wall stiffness and its impact on right ventricular afterload in patients with repaired tetralogy of fallot. *Ann Thorac Surg*. 2013. https://doi.org/10.1016/j.athoracsur.2013.05.085 PMID: 23972390
22. Van Wolferen SA, Marcus JT, Westerhof N, Spreeuwenberg MD, Marques KM, Bronzwaer JG, et al. Right coronary artery flow impairment in patients with pulmonary hypertension. *Eur Heart J*. 2008. https://doi.org/10.1093/eurheartj/ehm567 PMID: 18065750
23. Zong P, Tune JD, Setty S, Downey HF. Endogenous nitric oxide regulates right coronary blood flow during acute pulmonary hypertension in conscious dogs. *Basic Res Cardiol*. 2002. https://doi.org/10.1007/s003950200048 PMID: 12200639
24. Hsu S, Houston BA, Tampakakis E, Bacher AC, Rhodes PS, Mathai SC, et al. Right ventricular functional reserve in pulmonary arterial hypertension. *Circulation*. 2016. https://doi.org/10.1161/CIRCULATIONAHA.116.022082
25. Gómez A, Bialostozky D, Zajarias A, Santos E, Palomar A, Martínez ML, et al. Right ventricular ischemia in patients with primary pulmonary hypertension. *J Am Coll Cardiol*. 2001; 38(4):1137–1142. https://doi.org/10.1016/S0735-1097(01)01496-6 PMID: 11583894
26. Bruinsma P, Arts T, Dankelman J, Spaan JAE. Model of the coronary circulation based on pressure dependence of coronary resistance and compliance. *Basic Res Cardiol*. 1988. https://doi.org/10.1007/BF01906680
27. Razavi R, Hill DL, Keevil SF, Miquel ME, Muthurangu V, Hedge S, et al. Cardiac catheterisation guided by MRI in children and adults with congenital heart disease. *Lancet*. 2003. https://doi.org/10.1016/S0140-6736(03)14956-2
28. Silva Vieira M, Hussain T, Alberto Figueroa C. Patient-Specific Image-Based Computational Modeling in Congenital Heart Disease: A Clinician Perspective. *J Cardiol Ther*. 2015. https://doi.org/10.12970/2311-052X.2015.03.02.2
29. Xiao N, Humphrey JD, Figueroa CA. Multi-scale computational model of three-dimensional hemodynamics within a deformable full-body arterial network. *J Comput Phys*. 2013. https://doi.org/10.1016/j.jcp.2012.09.016 PMID: 23729840
30. Lau KD, Figueroa CA. Simulation of short-term pressure regulation during the tilt test in a coupled 3D–0D closed-loop model of the circulation. *Biomech Model Mechanobiol*. 2015. https://doi.org/10.1007/s10237-014-0645-x PMID: 25567754
31. Muzik O, Paridon SM, Singh TP, Morrow WR, Dayanikli F, Di Carli MF. Quantification of myocardial blood flow and flow reserve in children with a history of Kawasaki disease and normal coronary arteries using positron emission tomography. *J Am Coll Cardiol*. 1996.
32. Fullerton DA, Kirson LE, Jones SD, McIntyre RC. Adenosine is a selective pulmonary vasodilator in cardiac surgical patients. *Chest*. 1996. https://doi.org/10.1378/chest.109.1.41
33. Borgdorff MAJ, Dickinson MG, Berger RMF, Bartelds B. Right ventricular failure due to chronic pressure load: What have we learned in animal models since the NIH working group statement? *Heart Fail Rev*. 2015. https://doi.org/10.1007/s10741-015-9479-6 PMID: 25771982
34. Voelkel NF, Quaife RA, Leinwand LA, Barst RJ, McGoon MD, Meldrum DR, et al. Right ventricular function and failure: Report of a National Heart, Lung, and Blood Institute working group on cellular and molecular mechanisms of right heart failure. *Circulation*. 2006. https://doi.org/10.1161/CIRCULATIONAHA.106.632208 PMID: 17060398
35. Akasaka T, Yoshikawa J, Yoshida K, Hozumi T, Takagi T, Okura H. Comparison of relation of systolic flow of the right coronary artery to pulmonary artery pressure in patients with and without pulmonary hypertension. *Am J Cardiol*. 1996; 78(2):240–244. https://www.ncbi.nlm.nih.gov/pubmed/8712154. PMID: 8712154